Acta Crystallographica Section D
Biological Crystallography
ISSN 0907-4449

Structure of the corrinoid:coenzyme M methyltransferase MtaA from *Methanosarcina mazei*

Astrid Hoeppner,[a,b]‡ Frank Thomas,[c]‡ Alma Rueppel,[a] Reinhard Hensel,[c] Wulf Blankenfeldt,[d] Peter Bayer[a] and Annette Faust[e]*

[a]Structural and Medicinal Biochemistry, Centre of Medical Biotechnology (ZMB), University of Duisburg-Essen, Campus Essen, 45117 Essen, Germany, [b]Institute for Biochemical Plant Physiology, Heinrich-Heine-University, 40225 Düsseldorf, Germany, [c]Microbiology I, University of Duisburg-Essen, 45141 Essen, Germany, [d]Department of Biochemistry, University of Bayreuth, 95440 Bayreuth, Germany, and [e]Centre for Biochemistry and Molecular Biology (ZBM), Christian-Albrechts-University, 24118 Kiel, Germany

‡ These authors contributed equally to this work.

Correspondence e-mail: afaust@zbm.uni-kiel.de

Received 30 June 2012
Accepted 7 September 2012

PDB References: MtaA, 4ay7; SeMet-MtaA, 4ay8

The zinc-containing corrinoid:coenzyme M methyltransferase MtaA is part of the methanol–coenzyme M–methyltransferase complex of *Methanosarcina mazei*. The whole complex consists of three subunits: MtaA, MtaB and MtaC. The MtaB–MtaC complex catalyses the cleavage of methanol (bound to MtaB) and the transfer of the methyl group onto the cobalt of cob(I)alamin (bound to MtaC). The MtaA–MtaC complex catalyses methyl transfer from methyl-cob(III)alamin (bound to MtaC) to coenzyme M (bound to MtaA). The crystal structure of the MtaB–MtaC complex from *M. barkeri* has previously been determined. Here, the crystal structures of MtaA from *M. mazei* in a substrate-free but Zn^{2+}-bound state and in complex with Zn^{2+} and coenzyme M (HS-CoM) are reported at resolutions of 1.8 and 2.1 Å, respectively. A search for homologous proteins revealed that MtaA exhibits 23% sequence identity to human uroporphyrinogen III decarboxylase, which has also the highest structural similarity (r.m.s.d. of 2.03 Å for 306 aligned amino acids). The main structural feature of MtaA is a TIM-barrel-like fold, which is also found in all other zinc enzymes that catalyse thiol-group alkylation. The active site of MtaA is situated at the narrow bottom of a funnel such that the thiolate group of HS-CoM points towards the Zn^{2+} ion. The Zn^{2+} ion in the active site of MtaA is coordinated tetrahedrally *via* His240, Cys242 and Cys319. In the substrate-free form the fourth ligand is Glu263. Binding of HS-CoM leads to exchange of the O-ligand of Glu263 for the S-ligand of HS-CoM with inversion of the zinc geometry. The interface between MtaA and MtaC for transfer of the methyl group from MtaC-bound methylcobalamin is most likely to be formed by the core complex of MtaB–MtaC and the N-terminal segment (a long loop containing three α-helices and a β-hairpin) of MtaA, which is not part of the TIM-barrel core structure of MtaA.

1. Introduction

The physiological group methanoarchaea is characterized by a unique energy metabolism, methanogenesis, which is mainly responsible for the biogenic formation of the potent greenhouse gas methane (Deppenmeier, 2002). In all methanoarchaea, methylated coenzyme M (H_3C-S-CoM) serves as the terminal methyl-group carrier which is reductively cleaved to methane. Among the known genera of methanoarchaea, members of the genus *Methanosarcina* are the most versatile regarding the substrates used for formation of H_3C-S-CoM. In particular, *Methanosarcina* species can utilize methanol, methylated amines and methylated sulfides as well as acetate to form H_3C-S-CoM. In case of methanol, a soluble methyl-

transferase complex consisting of three subunits designated MtaB, MtaC and MtaA is involved in HS-CoM methylation. MtaB and MtaA are zinc-dependent enzymes (Sauer & Thauer, 1997). The first half-reaction is realised by the MtaB–MtaC complex, in which MtaB cleaves off methanol and transfers the resulting methyl carbocation to the MtaC-bound cob(I)alamin cofactor, forming methyl-cob(III)alamin. In the second half-reaction the complex MtaA–MtaC is established by a rearrangement of the corrinoid-carrying domain of MtaC. MtaA then catalyses the HS-CoM-dependent demethylation of the methyl-cob(III)alamin prosthetic group of MtaC, forming cob(I)alamin and H_3C-S-CoM (Sauer & Thauer, 2000) (Fig. 1). However, when methylated amines or dimethylsulfides instead of methanol are converted into methane, the HS-CoM methylation is catalysed by isoenzymes of MtaA: MtbA and MtsA. The Zn^{2+} sites of MtaA and MtbA have been analysed by X-ray absorption spectroscopy (Krüer *et al.*, 2002; Gencic *et al.*, 2001).

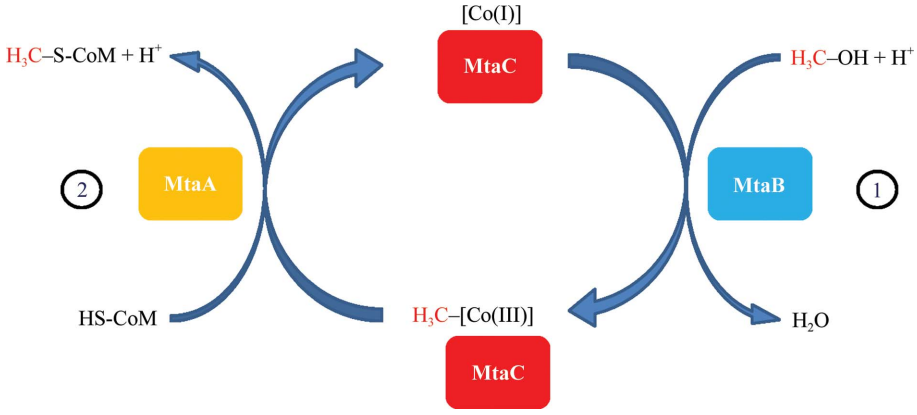

Figure 1
Schematic representation of the reactions catalysed by the methanol–coenzyme M–methyltransferase complex of *M. mazei*.

Structural analysis of the MtaB–MtaC complex from *M. barkeri* has previously been published, giving insights into the biological activation of methanol (Hagemeier *et al.*, 2006). With the three-dimensional structure of MtaA from *M. mazei* presented here, all of the enzymes involved in the conversion of methanol to methane in *Methanosarcina* species have now been characterized in atomic detail.

2. Materials and methods

2.1. Cloning and protein expression

The full-length *mtaA1* gene from *M. mazei* (accession No. NP_633094) was amplified from genomic *M. mazei* DNA using a proof-reading DNA polymerase (recombinant *Pfu* DNA Polymerase, Fermentas Life Science, St Leon-Rot, Germany) and the following primer pair: forward, 5′-CGC GGA ATT **CAT ATG** ACC GAT ATG AGC GAA TTC-3′; reverse, 5′-AGA GCG GAT **CCT CGA G**TC AGG CGT AGA ATT C-3′. The amplified sequence was cloned into vector pET-15b using DNA fragments pre-digested with the restriction nucleases *Nde*I and *Xho*I. Restriction sites were introduced upstream and downstream of *mtaA1 via* the used primer pair (restriction recognition sites are shown in bold). *Escherichia coli* BL21 (DE3) cells (Novagen, Darmstadt, Germany) were transformed with the derived construct pET15b+MM_1070, allowing the expression of MtaA with an N-terminal His_6 tag. In order to label MtaA with selenomethionine (SeMet), the methionine-pathway inhibition method was used (Doublié, 1997; Walden, 2010). His_6-tagged native and SeMet-derivatized MtaA were purified by affinity chromatography on an Ni–NTA column (Qiagen, Hilden, Germany) and size-exclusion chromatography on a Superdex 200 HiLoad 26/60 column (GE Healthcare, Freiburg, Germany). Specific enzyme activity was determined by HS-CoM-dependent demethylation of methyl-cob(III)alamin as described previously (Grahame, 1989).

2.2. Crystallization and data collection

Crystals of His_6-tagged MtaA were obtained at room temperature by the hanging-drop vapour-diffusion method using drops consisting of 1 µl protein solution at 8 mg ml^{-1} in 25 m*M* HEPES pH 7.0, 10 m*M* NaCl, 3% glycerol, 10 m*M* DTT and 1 µl reservoir solution equilibrated against 500 µl reservoir solution. The reservoir solution consisted of 0.1 *M* Tris pH 8.5, 0.2 *M* $MgCl_2$, 30% PEG 4000, 2% 1,1,1,3,3,3-hexafluoro-2-propanol. Crystals appeared after 1–2 d. The crystals were cryocooled in mother liquor supplemented with 30% glycerol prior to flash-cooling in liquid N_2. Diffraction data were collected with a PILATUS 6M detector on beamline X10SA at the Swiss Light Source (SLS), Paul Scherrer Institute, Villigen, Switzerland using a wavelength of 0.9786 Å (12.68 keV). These crystals grew to approximate dimensions of 250 × 25 × 10 µm, belonged to space group $P2_1$, with unit-cell parameters a = 44.2, b = 167.4, c = 45.8 Å, β = 117.4°, and diffracted X-rays to 1.8 Å resolution. Hexagonal-shaped crystals of the selenomethionine derivative were obtained by the sitting-drop vapour-diffusion method, in which drops consisting of 1 µl protein solution (6 mg ml^{-1} protein in 25 m*M* HEPES pH 7.0, 10 m*M* NaCl, 3% glycerol, 10 m*M* DTT containing 2 m*M* HS-CoM incubated for 90 min at 293 K) and 1 µl reservoir solution (100 m*M* MES pH 6.5, 65% MPD) were equilibrated against 500 µl reservoir solution at 293 K. These crystals belonged to space group $P3_2$, with unit-cell parameters a = 125.1, c = 38.8 Å and grew within 22 d to final dimensions of 105 × 65 × 50 µm. Prior to the diffraction experiment, the crystals were mounted in reservoir solution and flash-cooled in liquid nitrogen. Diffraction data were collected using a MAR165 CCD detector on BL14.3 operated by the Joint Berlin MX Laboratory at the BESSY II electron-storage ring (Berlin-Adlershof, Germany; Mueller *et al.*, 2012) at 0.896 Å (13.86 keV). In all cases, diffraction data were

indexed and integrated using *XDS* (Kabsch, 2010) and scaled using *SCALA* (Evans, 2006). Calculation of the Matthews coefficient (Matthews, 1968) indicated two MtaA molecules per asymmetric unit in both crystal forms. Data-collection statistics are summarized in Table 1.

Table 1
Statistics of data collection, processing and structure refinement.

Values in parentheses are for the highest resolution bin. Each data set was collected from one single crystal.

	Apo MtaA	SeMet-MtaA
Data collection		
Source	X10SA, SLS	BL14.3, BESSY II
Space group	$P2_1$	$P3_2$
Unit-cell parameters (Å, °)	a = 44.2, b = 167.4, c = 45.9, $\alpha = \gamma = 90$, $\beta = 117.4$	$a = b$ = 125.2, c = 38.9, $\alpha = \beta = 90$, $\gamma = 120$
Resolution (Å)	42–1.8 (1.9–1.8)	38.9–2.1 (2.2–2.1)
$R_{merge}/R_{p.i.m.}$† (%)	11.1 (78.6)/5.5 (39.6)	7.4 (20.3)/4.3 (13.9)‡
Mean $I/\sigma(I)$	8.1 (2.2)	30.8 (10.4)
Completeness (%)	100 (100)	99.8 (99.8)
Multiplicity	4.8 (4.8)	7.6 (4.7)
Refinement		
Resolution (Å)	42–1.8 (1.85–1.80)	38.9–2.1 (2.16–2.10)
No. of reflections	51799 (4006)	37708 (2755)
R_{work}/R_{free} (%)	16.3 (27.0)/21.3 (33.0)	14.9 (20.1)/18.1 (25.1)
No. of atoms		
Protein (chain *A*/chain *B*)	2510/2526	2525/2525
Zn^{2+}	2	2
Mg^{2+}	2	—
HS-CoM	—	2
Ligands	—	3
Water	408	369
B factors (Å^2)		
Protein (chain *A*/chain *B*)	25.4/26.7§	10.0/9.9
Zn^{2+}	48.7¶	17.2
Mg^{2+}	40.3¶	—
HS-CoM	—	14.9
Ligands	—	38.3
Water	33.7	16.2
R.m.s. deviations		
Bond lengths (Å)	0.019	0.009
Bond angles (°)	1.965	1.182
MolProbity clashscore	5.81 [94th percentile]	4.13 [99th percentile]
Ramachandran favoured/outliers (%)	97.90/0.45	97.33/0.45
MolProbity score	1.42 [96th percentile]	1.32 [99th percentile]
PDB code	4ay7	4ay8

† $R_{p.i.m.} = \sum_{hkl}\{1/[N(hkl)-1]\}^{1/2}\sum_i |I_i(hkl) - \langle I(hkl)\rangle|/\sum_{hkl}\sum_i I_i(hkl)$, where N is the number of observations of the reflection with index hkl (Weiss, 2001). ‡ Data-collection statistics for SAD data refer to unmerged Friedel pairs. § Average *B* factors include TLS parameters for the apo MtaA data set. ¶ Despite the higher mobility of zinc in the unbound state, the high *B* factors for Zn^{2+} and Mg^{2+} might also be the result of incomplete occupancy of these binding sites.

2.3. Structure determination

The structure of SeMet-MtaA was solved from the anomalous data of the $P3_2$ crystal form using the SAS protocol (run in the advanced version) of *Auto-Rickshaw*, the EMBL Hamburg automated crystal structure-determination platform (Panjikar *et al.*, 2005, 2009), with various programs from the *CCP*4 program suite (Winn *et al.*, 2011), *SHELXC*/*D*/*E* (Schneider & Sheldrick, 2002; Sheldrick, 2008) for phasing, *APS* (Hao, 2004) and *DM* (Cowtan, 1994) for density modification, *ARP*/*wARP* (Morris *et al.*, 2004; Perrakis *et al.*, 1999) for model building and *CNS* (Brünger *et al.*, 1998; Brunger, 2007) and *REFMAC*5 (Murshudov *et al.*, 2011) for refinement. Detailed information of the structure solution can be found in the Supplementary Material[1]. The model was subsequently completed by iterative manual inspection and model advancement in *Coot* (Emsley & Cowtan, 2004; Emsley *et al.*, 2010) followed by refinement in *REFMAC*5.

The refined model was used as a starting model to interpret the diffraction data of the $P2_1$ crystals of MtaA, employing *MOLREP* (Vagin & Teplyakov, 2010) from the *CCP*4 program suite for molecular replacement. The resulting model was subsequently refined using *Coot* and *REFMAC*5 as described above. The three-dimensional models of MtaA and SeMet-MtaA were validated using *PROCHECK* (Laskowski *et al.*, 1993), *SFCHECK* (Vaguine *et al.*, 1999) and *MolProbity* (Chen *et al.*, 2010; Davis *et al.*, 2007). Refinement statistics are summarized in Table 1.

Electrostatic surface potentials were calculated using the program *DelPhi* (Rocchia *et al.*, 2001; Gilson & Honig, 1988; Gilson *et al.*, 1988; Honig & Nicholls, 1995; Klapper *et al.*, 1986; Nicholls & Honig, 1991; Yang *et al.*, 1993). Structural homologues were identified by *PDBeFold* (Krissinel & Henrick, 2004). All visualization and preparation of structural images was performed with *PyMOL* (DeLano, 2002). Modelling was performed in *CHIMERA* (Pettersen *et al.*, 2004).

[1] Supplementary material has been deposited in the IUCr electronic archive (Reference: YT5046). Services for accessing this material are described at the back of the journal.

3. Results and discussion

3.1. Overall structure of MtaA

Two distinct protein chains (*A* and *B*) were identified in the electron density of the $P3_2$ crystal form of SeMet-MtaA. In both protein chains the eight N-terminal residues could not be traced. Each chain contained 340 amino acids. The $P2_1$ MtaA crystals also contained two protein chains in the asymmetric unit, the 11 N-terminal residues of which were not visible. Overall, all of the chains were structurally very similar, with r.m.s.d.s between 0.2 and 0.5 Å. Crystal-packing analysis indicated that MtaA was a monomer, with a contact area between monomers of 253 Å^2 for the substrate-bound MtaA crystals and 173 Å^2 for the substrate-free crystals (calculated

using *PISA*; Krissinel, 2010; Krissinel & Henrick, 2005, 2007), which was in agreement with the results from size-exclusion chromatography. MtaA exhibited a TIM-barrel-like three-dimensional structure similar to the $(\alpha/\beta)_8$ barrel as represented, for example, by chicken triosephosphate isomerase (PDB entry 1tim; Banner *et al.*, 1976). As the TIM-barrel fold is widespread in nature throughout almost all classes of enzymes, the sequential arrangement of the secondary-structure elements that build up the barrel structure can vary (see Supplementary Fig. S1*a*). In addition to the TIM-barrel-like fold, MtaA comprises an N-terminal structural motif composed of three helices (α_1–α_3) and one antiparallel β-sheet with two strands (β_2 and β_3). In the structure of substrate-bound MtaA, HS-CoM is positioned on the C-terminal side of the barrel (Fig. 2).

3.2. Structural homologues and putative complex of MtaA and the MtaC Rossmann domain

Human uroporphyrinogen III decarboxylase (PDB entry 1r3q; Phillips *et al.*, 2003) is the closest structural homologue of MtaA, with an r.m.s.d. of 2.03 Å for 306 aligned amino acids of MtaA as calculated by *PDBeFold* (Krissinel & Henrick, 2004). Uroporphyrinogen III decarboxylase contains the same additional N-terminal segment as MtaA (Fig. 2*b*). However, uroporphyrinogen III decarboxylase is not a zinc-dependent enzyme and it catalyses a reaction that differs from that catalysed by MtaA. The position of the porphyrin-ring system in uroporphyrinogen III decarboxylase is at the bottom of a shallow tunnel shielded by the N-terminal segment. The active site of MtaA is situated at the bottom of a shallow funnel on the C-terminal side of the TIM-barrel-like fold. The funnel narrows to allow HS-CoM to bind (Fig. 2*b*). Comparison of the surface cavities in uroporphyrinogen III decarboxylase and MtaA shows that the cavity in MtaA is deeper and narrower and is restricted by the N-terminal segment which caps the active centre of MtaA. Overall, the structural homology between MtaA and uroporphyrinogen III decarboxylase thus reflects the binding of similar substrates, *i.e.* porphyrin derivatives, not a similarity in catalytic activity. Nevertheless, the position of uroporphyrinogen in the structure of uroporphyrinogen III decarboxylase can be used as an initial starting point for the proposed binding site for the methyl-cob(III)amine of MtaC during complex formation with MtaA. Furthermore, the highly negative electrostatic surface of the active centre of MtaA, which is also found in MtaB, is an additional hint to the potential binding position of the corrinoid upon MtaC binding. The structure of the MtaB–MtaC complex (Hagemeier *et al.*, 2006) and the arrangement of the two subunits of the recently determined complex structure of corrinoid iron–sulfur protein (CFeSP) in complex with its methyltransferase (MeTr) from the acetogenic bacterium *Moorella thermoacetica* (Kung *et al.*, 2012) have been taken into account in modelling the complex between the Rossmann domain of MtaC and MtaA. The model was built manually using all of the above considerations and a slight rotation and translation so that there were no sterical clashes between MtaA and the Rossmann domain of MtaC (Fig. 3). The N-terminal segment of MtaA is most likely to be involved in the formation of the interface between MtaA and the Ross-

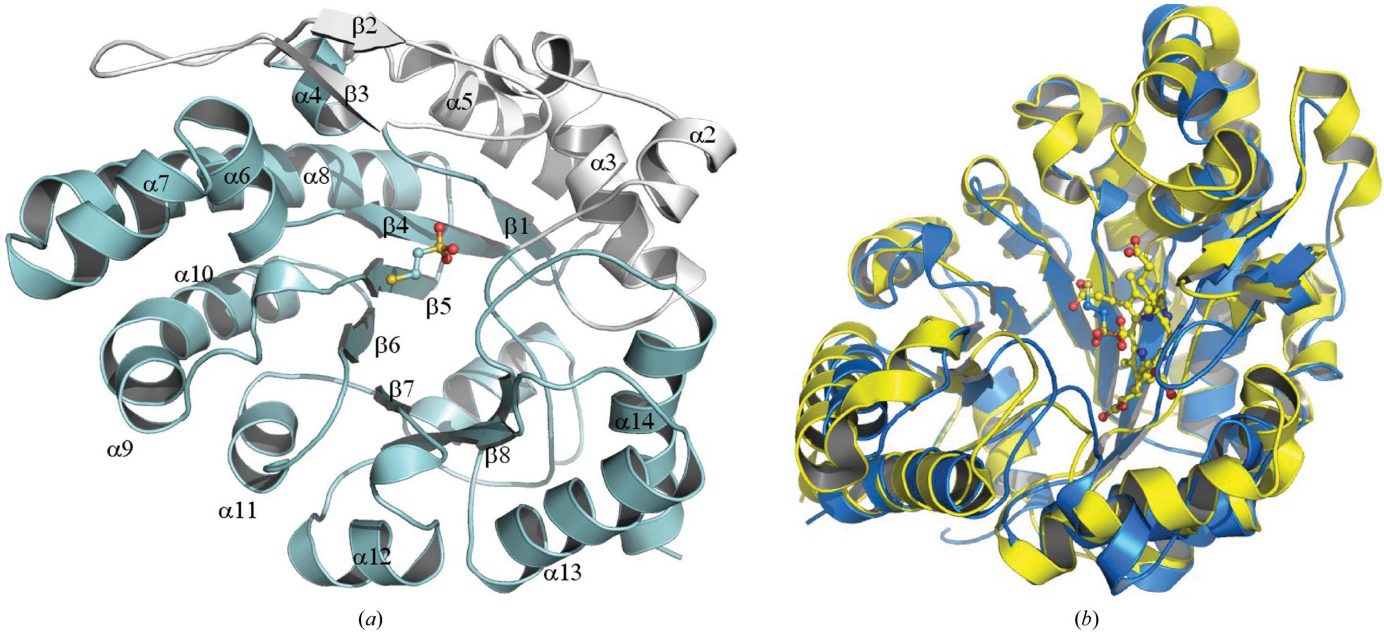

Figure 2
(*a*) Ribbon representation of an MtaA molecule with bound HS-CoM. The TIM-barrel-like fold is shown in light blue and the additional N-terminal secondary-structure elements are shown in white. HS-CoM is shown in ball-and-stick representation; C atoms are coloured light blue, O atoms red and S atoms yellow. The numbering of the secondary-structure elements is consistent with that of the structural alignment with uroporphyrinogen III decarboxylase (see Supplementary Fig. S1). (*b*) Superposition of MtaA (blue) with human uroporphyrinogen III decarboxylase (yellow; PDB entry 1r3q). Uroporphyrinogen and HS-CoM are shown in ball-and-stick representation.

mann domain of MtaC carrying the methyl-cob(III)amin and the core complex of MtaB–MtaC.

MtaA shares 45% sequence identity with its isoenzyme MtbA (Wu *et al.*, 2003) but has no identity to other Zn^{2+}-dependent enzymes that catalyze thiol-group alkylation (Harms & Thauer, 1996; Krüer *et al.*, 2002; LeClerc & Grahame, 1996). Despite their lack of sequence identity, all thiol-group-alkylating enzymes have a common TIM-barrel-like fold. Structural comparison with two of these enzymes resulted in an r.m.s.d. of 2.57 Å for 300 aligned amino acids of the N-terminal domain of the cobalamin-dependent methionine synthase (MetH) from *Thermatoga maritima* and an r.m.s.d. of 4.13 Å for 193 aligned amino acids of the C-terminal domain of the cobalamin-independent methionine synthase (MetE) from *T. maritima* (Koutmos *et al.*, 2008). Both enzymes catalyse the transfer of a methyl group from methyltetrahydrofolate to L-homocysteine to form methionine.

3.3. Active site and substrate binding

3.3.1. Zinc coordination. For zinc, a mainly covalent bond type to the coordinating atoms has been reported (Harding *et al.*, 2010), especially if the coordinating atoms are the N atoms of histidine or the sulfur anion of cysteine. In one molecule (chain *B*), the active site of the substrate-free MtaA structure shows tetrahedral coordination of Zn^{2+} by His240 (with a distance of 2.2 Å), Cys242 (2.8 Å), Cys319 (2.4 Å) and Glu263 (2.4 Å to O1 of the carboxy group). O1 of the carboxy group of Glu263 also forms a hydrogen bond to the main-chain N atom of Glu243 (3.0 Å), whereas O2 does not show any hydrogen-bond contacts. In chain *A* of this structure the Zn^{2+} ion is coordinated exactly as in the substrate-bound structure, with the fourth ligand missing as the side chain of Glu263 is moved away as in the substrate-bound structure. Here, hydrogen bonds are formed from the carboxyl O1 atom to the main-chain N atom of Glu243 (with a distance of 2.8 Å) and the ε-amino group of Lys265 (2.7 Å) and from the carboxyl O2 atom to the the ε-amino group of Lys265 (2.7 Å) and a water molecule (HOH 2167; 3.0 Å). In the crystal structure of substrate-bound MtaA the fourth Zn^{2+} ligand is the thiol group of HS-CoM instead of the O-ligand of Glu263. O1 of Glu263 is hydrogen-bonded, as in the substrate-free structure, to the main-chain N atom of Glu243 (with a distance of 2.8 Å) and a water molecule (2.6 Å) and O2 is hydrogen-bonded to two water molecules (2.8 and 3.0 Å). In the substrate-bound structure the distances between the S atoms and Zn^{2+} are all 2.4 Å and the distance between the N atom and Zn^{2+} is 2.1 Å (Figs. 4*c* and 4*d*). Upon substrate binding, the relative position of the Zn^{2+} ion remains the same in chain *A* and shifts 1.6 Å compared with its position in chain *B* of the substrate-free structure (Fig. 4*d*). All coordinating distances are within the range of distances reported for zinc-binding proteins (Harding *et al.*, 2010).

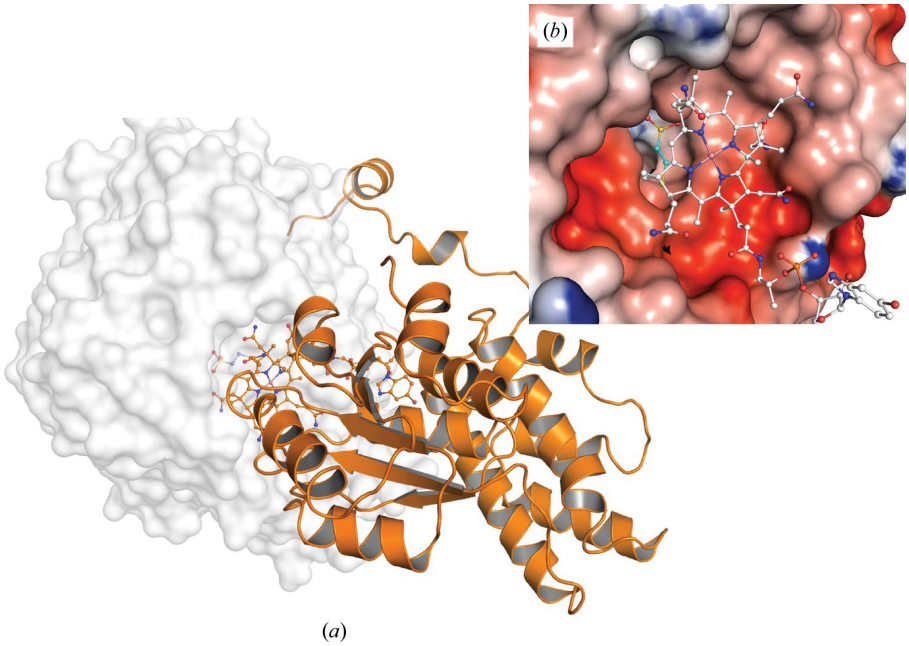

Figure 3
(*a*) Putative complex of MtaA and the Rossmann domain of MtaC. MtaA is shown as a surface representation in white and the Rossmann domain of MtaC is shown as a ribbon representation. HS-CoM and cob(III)alamin are shown in ball-and-stick representation. (*b*) Close-up of the putative corrinoid-binding position in HS-CoM-bound MtaA. The surface of MtaA is coloured according to the electrostatic potential, which was calculated with *DelPhi* (Rocchia *et al.*, 2001; Gilson & Honig, 1988; Gilson *et al.*, 1988; Honig & Nicholls, 1995; Klapper *et al.*, 1986; Nicholls & Honig, 1991; Yang *et al.*, 1993) using the default input parameters. The colour scale is from $-10kT$/e (red) to $+10kT$/e (blue). The cob(I)alamin molecule was modelled manually inside the active-site entrance. The cob(I)alamin molecule is shown in white as a stick model, the C atoms of the substrate HS-CoM are shown in cyan and the individual atoms are coloured according to atom type (blue for nitrogen, red for oxygen and yellow for sulfur) as ball-and-stick models.

3.3.2. CoM coordination and substrate specificity. At physiological pH it is expected that Zn^{2+} will replace the H^+ on the thiol group of cysteine (Harding *et al.*, 2010). The finding that a proton is released upon binding of HS-CoM to MtbA (Gencic *et al.*, 2001) suggests that HS-CoM binds Zn^{2+} in the thiolate form. In addition to the coordination of the thiolate group by Zn^{2+}, two of the sulfonate O atoms are hydrogen-bonded *via* Gln97 (with a distance of 3 Å) and Gln32 (2.9 Å). The HS-CoM is oriented horizontally on top of the TIM barrel and is exposed to the protein surface, with the thiolate group of HS-CoM pointing towards the zinc (Figs. 2, 4*a* and 4*b*). As indicated by the low r.m.s.d.s for the substrate-free and substrate-bound structures, the protein backbone remains rigid. The distance between the sulfonate-binding site and the

Zn^{2+} ion determines the substrate specificity of MtaA. As pointed out by LeClerc & Grahame (1996), catalytic activity of MtaA and MtbA from *M. barkeri* was found in the presence of HS-CoM, 3-mercaptopropionic acid and 2-thioethane phosphonic acid, but not with thiols with longer or shorter carbon chains, suggesting the necessity of a free sulfhydryl group at a specific distance from an anionic acid group. Sequence comparisons with other methyl-*X* coenzyme M methyltransferases (Fig. 5) show that in addition to the zinc-binding motif, the amino acids that coordinate the sulfonate group are also highly conserved.

The role of zinc is postulated to be that of a Lewis acid that activates the thiol group, thereby allowing alkylation by lowering the microscopic pK_a value from >9 to <7. This increases the nucleophilicity of HS-CoM and enables its attack on the methyl group of methyl-cob(III)alamin (Sauer & Thauer, 2000).

3.4. Zinc-binding motif and substrate activation by metal active-site elasticity

The zinc-binding motif of MtaA from *M. mazei* is His-*X*-Cys-X_{20}-Glu-X_{55}-Cys. The general motif His-*X*-Cys-X_n-Glu-X_m-Cys is also found in MtaA from *M. barkeri*, *M. acetovorans* and *Moorella thermoacetica* (Das *et al.*, 2007); MtbA from *M. barkeri* (Sauer & Thauer, 1997; Gencic *et al.*, 2001); MtsA from *M. mazei* and *M. barkeri* (Tallant *et al.*, 2001); and MetE from various species [PDB entries 1xdj (*Thermotoga maritima*; Pejchal & Ludwig, 2005), 1u1j (*Arabidopsis thaliana*; Ferrer *et al.*, 2004) and 3lzr (*Streptococcus mutans*; Fu *et al.*, 2011)]. In MtbA and MtsA the Glu is replaced by a highly conserved Asp (Fig. 5). In MetH from *T. maritima* a third Cys coordinates the zinc instead of a histidine and an asparagine is the fourth ligand in the substrate-free state (Koutmos *et al.*, 2008).

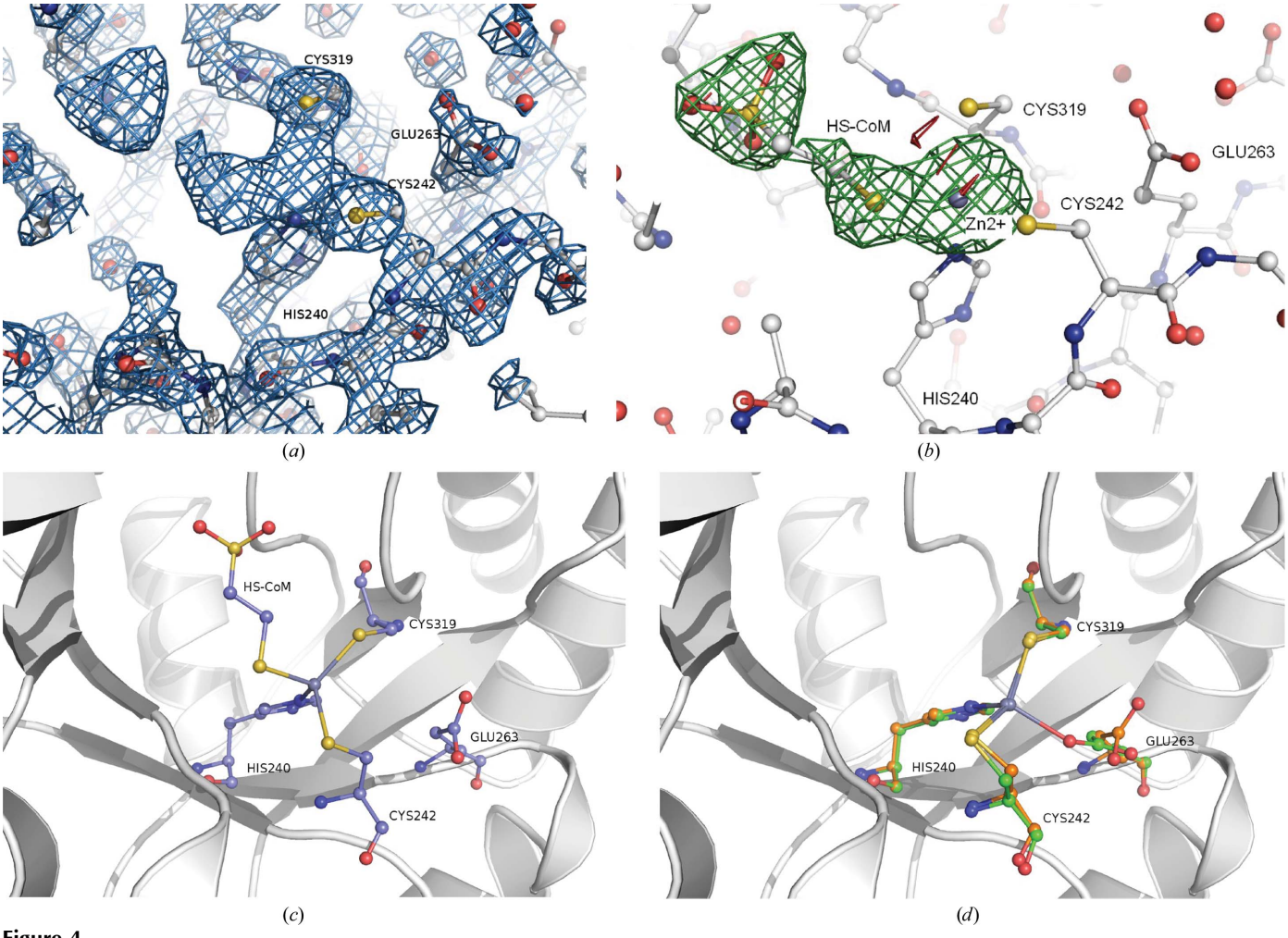

Figure 4
(*a*) Representative ($2F_o - F_c$, α_c) electron-density map detail around the active-site residues of substrate-bound MtaA before adding Zn^{2+} and HS-CoM to the model. The map is contoured at 1.5σ. (*b*) Representative ($F_o - F_c$, α_c) electron-density map detail around the active-site residues of substrate-bound MtaA before adding Zn^{2+} and HS-CoM to the model. The map is contoured at 5σ. Green represents positive difference density and red represents negative difference density. HS-CoM, which was added in a later refinement step, is shown as a ball-and-stick model. C atoms are coloured white, N atoms blue, O atoms red and S atoms yellow. (*c*, *d*) Zn^{2+} coordination in the active sites of (*c*) substrate-bound MtaA (blue) and (*d*) substrate-free MtaA (chain *B* in orange, chain *A* in green). The protein main chains are shown as ribbons. The coordinating side-chain residues are shown in ball-and-stick representation. O atoms are coloured red, N atoms blue, S atoms yellow and zinc ions grey.

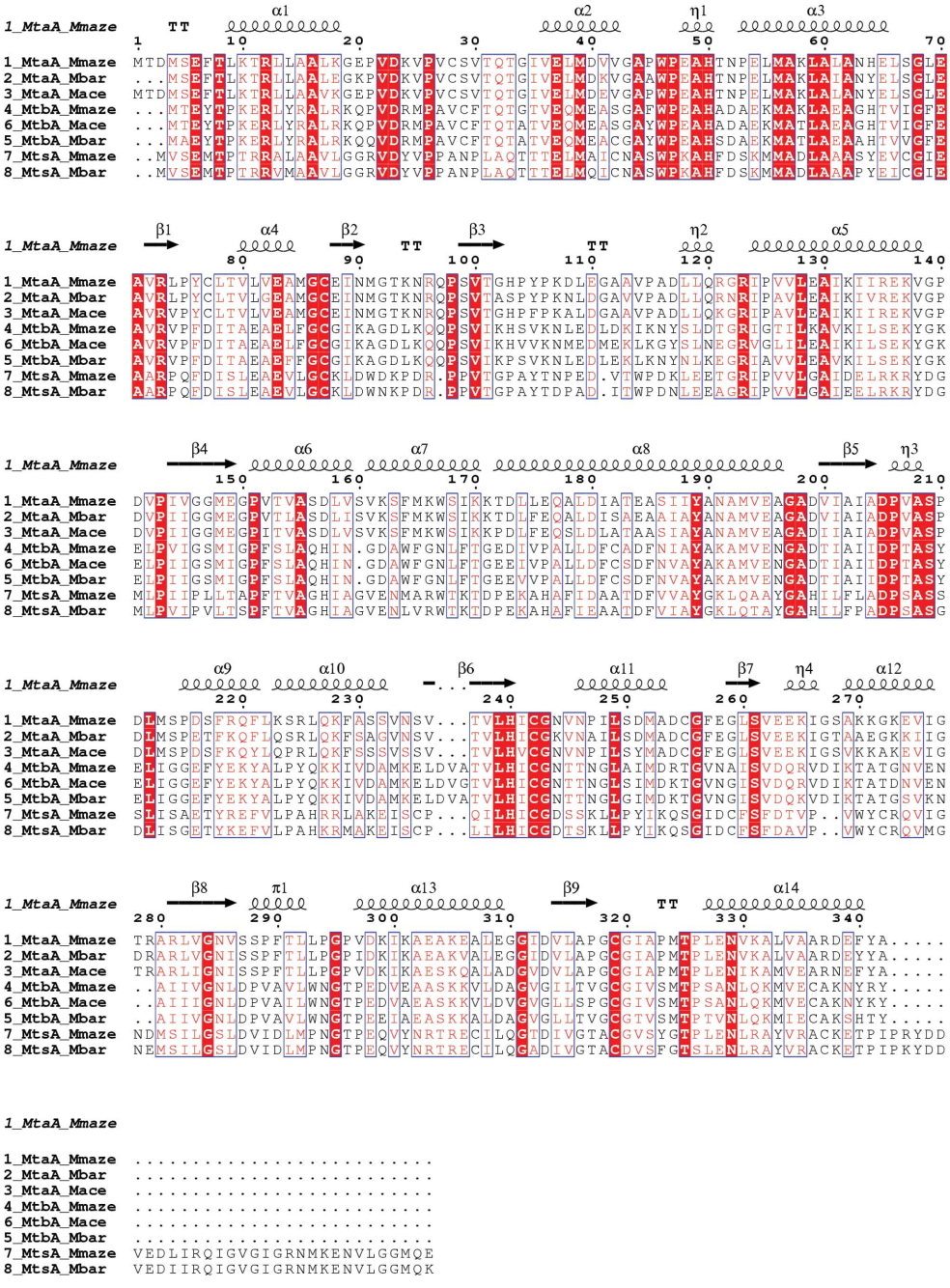

Figure 5
Sequence alignment of MtaA from various *Methanosarcina* species and its isoenzymes MtbA and MtsA (Matthews *et al.*, 2008 and references therein). The sequence alignment was performed with *ClustalW* v.2.0 (Larkin *et al.*, 2007). The final figure was prepared with the program *ESPript* (Gouet *et al.*, 1999) using a similarity score of '0.7 0.5 B'.

Despite their lack of sequence identity, the structures of the corrinoid-independent methionine synthase MetE from *S. mutans* (Fu *et al.*, 2011) show exactly the same features as that of MtaA. From the structures of MetE and MetH from *T. maritima* (Koutmos *et al.*, 2008), two models for the zinc inversion were proposed: an induced-fit model in which the binding of the substrate leads to conformational changes that facilitates zinc displacement or a dynamic equilibrium model in which zinc oscillates between the two tetrahedral geometries through a trigonal-bipyramidal intermediate even in the absence of zinc. The favoured dynamic-zinc model was further supported by the finding of Fu *et al.* (2011) that even in the absence of substrate the zinc together with Glu can adopt the substrate-bound conformation. In chain *A* of substrate-free MtaA the Zn^{2+} ion is coordinated exactly as in the substrate-bound structure, with the fourth ligand missing (Figs. 4*c* and 4*d*). The *B* factors of zinc in the substrate-free structure are also unusually high, indicating that the Zn^{2+} ion is more mobile than in the substrate-bound state. The different coordinations of Zn^{2+} in the two molecules and its increased mobility also favour the dynamic equilibrium model for MtaA.

4. Conclusions

Crystal structures of MtaA from *M. mazei* in the resting state and the substrate-bound state have been determined to resolutions of 1.8 and 2.1 Å, respectively. The closest structural homologue to MtaA is uroporphyrinogen III decarboxylase, which is not a zinc-dependent enzyme, but the binding of its substrate might resemble the position of methylcob(III)amin bound to the Rossmann domain of MtaC in the MtaA–MtaC complex. This information has been used together with further structural information on the MtaB–MtaC complex of *M. barkeri* (Hagemeier *et al.*, 2006) and on the complex structure of corrinoid iron–sulfur protein (CFeSP) with its methyltransferase MeTr from *Moorella thermoacetica* (Kung *et al.*, 2012) to model the complex between MtaA and the Rossmann domain of MtaC. It is most likely that the interface between MtaA and MtaC is primarily formed by the core complex of MtaB–MtaC and the N-terminal segment of MtaA.

Despite the lack of overall sequence identity, MtaA and MetE share the same zinc-coordination motif and the same features upon substrate binding and coordination of zinc in

the resting state. Structural information on MtaA as well as on MetE and MetH (Koutmos *et al.*, 2008; Datta *et al.*, 2008; Fu *et al.*, 2011; Matthews *et al.*, 2008; Matthews, 2009) favours the dynamic equilibrium model over the induced-fit model for MtaA.

We gratefully acknowledge financial support from the HZB. We also thank the HZB for the allocation of synchrotron-radiation beamtime and the beamline staff of HZB (Berlin, Germany) and PSI (Villigen, Switzerland) for their support.

References

Banner, D. W., Bloomer, A., Petsko, G. A., Phillips, D. C. & Wilson, I. A. (1976). *Biochem. Biophys. Res. Commun.* **72**, 146–155.

Brunger, A. T. (2007). *Nature Protoc.* **2**, 2728–2733.

Brünger, A. T., Adams, P. D., Clore, G. M., DeLano, W. L., Gros, P., Grosse-Kunstleve, R. W., Jiang, J.-S., Kuszewski, J., Nilges, M., Pannu, N. S., Read, R. J., Rice, L. M., Simonson, T. & Warren, G. L. (1998). *Acta Cryst.* D**54**, 905–921.

Chen, V. B., Arendall, W. B., Headd, J. J., Keedy, D. A., Immormino, R. M., Kapral, G. J., Murray, L. W., Richardson, J. S. & Richardson, D. C. (2010). *Acta Cryst.* D**66**, 12–21.

Cowtan, K. (1994). *Jnt CCP4/ESF–EACBM Newsl. Protein Crystallogr.* **31**, 34–38.

Das, A., Fu, Z., Tempel, W., Liu, Z., Chang, J., Chen, L., Lee, D., Zhou, W., Xu, H., Shaw, N., Rose, J. P., Ljungdahl, L. G. & Wang, B. (2007). *Proteins Struct. Funct. Bioinformat.* **1**, 167–176.

Datta, S., Koutmos, M., Pattridge, K. A., Ludwig, M. L. & Matthews, R. G. (2008). *Proc. Natl Acad. Sci. USA*, **105**, 4115–4120.

Davis, I. W., Leaver-Fay, A., Chen, V. B., Block, J. N., Kapral, G. J., Wang, X., Murray, L. W., Arendall, W. B. III, Snoeyink, J., Richardson, J. S. & Richardson, D. C. (2007). *Nucleic Acids Res.* **35**, W375–W383.

DeLano, W. L. (2002). *PyMOL*. http://www.pymol.org.

Deppenmeier, U. (2002). *Prog. Nucleic Acid Res. Mol. Biol.* **71**, 223–283.

Doublié, S. (1997). *Methods Enzymol.* **276**, 523–530.

Emsley, P. & Cowtan, K. (2004). *Acta Cryst.* D**60**, 2126–2132.

Emsley, P., Lohkamp, B., Scott, W. G. & Cowtan, K. (2010). *Acta Cryst.* D**66**, 486–501.

Evans, P. (2006). *Acta Cryst.* D**62**, 72–82.

Ferrer, J.-L., Ravanel, S., Robert, M. & Dumas, R. (2004). *J. Biol. Chem.* **43**, 44235–44238.

Fu, T.-M., Almqvist, J., Liang, Y.-H., Li, L., Huang, Y. & Su, X.-D. (2011). *J. Mol. Biol.* **412**, 688–697.

Gencic, S., LeClerc, G. M., Gorlatova, N., Peariso, K., Penner-Hahn, J. E. & Grahame, D. A. (2001). *Biochemistry*, **40**, 13068–13078.

Gilson, M. K. & Honig, B. (1988). *Proteins*, **4**, 7–18.

Gilson, M. K., Sharp, K. A. & Honig, B. H. (1988). *J. Comput. Chem.* **9**, 327–335.

Gouet, P., Courcelle, E., Stuart, D. I. & Métoz, F. (1999). *Bioinformatics*, **15**, 305–308.

Grahame, D. A. (1989). *J. Biol. Chem.* **264**, 12890–12894.

Hagemeier, C. H., Krueer, M., Thauer, R. K., Warkentin, E. & Ermler, U. (2006). *Proc. Natl Acad. Sci. USA*, **103**, 18917–18922.

Hao, Q. (2004). *J. Appl. Cryst.* **37**, 498–499.

Harding, M. M., Nowicki, M. W. & Walkinshaw, M. D. (2010). *Crystallogr. Rev.* **16**, 247–302.

Harms, U. & Thauer, R. K. (1996). *Eur. J. Biochem.* **235**, 653–659.

Honig, B. & Nicholls, A. (1995). *Science*, **268**, 1144–1149.

Kabsch, W. (2010). *Acta Cryst.* D**66**, 125–132.

Klapper, I., Hagstrom, R., Fine, R., Sharp, K. & Honig, B. (1986). *Proteins*, **1**, 47–59.

Koutmos, M., Pejchal, R., Bomer, T. M., Matthews, R. G., Smith, J. L. & Ludwig, M. L. (2008). *Science*, **9**, 3286–3291.

Krissinel, E. (2010). *J. Comput. Chem.* **31**, 133–143.

Krissinel, E. & Henrick, K. (2004). *Acta Cryst.* D**60**, 2256–2268.

Krissinel, E. & Henrick, K. (2005). *CompLife 2005*, edited by M. R. Berthold, R. Glen, K. Diederichs, O. Kohlbacher & I. Fischer, pp. 67–78. Berlin/Heidelberg: Springer-Verlag.

Krissinel, E. & Henrick, K. (2007). *J. Mol. Biol.* **372**, 774–797.

Krüer, M., Haumann, M., Meyer-Klaucke, W., Thauer, R. K. & Dau, H. (2002). *Eur. J. Biochem.* **269**, 2117–2123.

Kung, Y., Ando, N., Doukov, T. I., Blasiak, L. C., Bender, G., Seravalli, J., Ragsdale, S. W. & Drennan, C. L. (2012). *Nature (London)*, **484**, 265–269.

Larkin, M. A., Blackshields, G., Brown, N. P., Chenna, R., McGettigan, P. A., McWilliam, H., Valentin, F., Wallace, I. M., Wilm, A., Lopez, R., Thompson, J. D., Gibson, T. J. & Higgins, D. G. (2007). *Bioinformatics*, **23**, 2947–2948.

Laskowski, R. A. (2001). *Nucleic Acids Res.* **29**, 221–222.

Laskowski, R. A. (2007). *Bioinformatics*, **23**, 1824–1827.

Laskowski, R. A. (2009). *Nucleic Acids Res.* **37**, D355–D359.

Laskowski, R. A., Chistyakov, V. V. & Thornton, J. M. (2005). *Nucleic Acids Res.* **33**, D266–D268.

Laskowski, R. A., Hutchinson, E. G., Michie, A. D., Wallace, A. C., Jones, M. L. & Thornton, J. M. (1997). *Trends Biochem. Sci.* **22**, 488–490.

Laskowski, R. A., Moss, D. S. & Thornton, J. M. (1993). *J. Mol. Biol.* **231**, 1049–1067.

LeClerc, G. M. & Grahame, D. A. (1996). *J. Biol. Chem.* **271**, 18725–18731.

Matthews, B. W. (1968). *J. Mol. Biol.* **33**, 491–497.

Matthews, R. G. (2009). *Met. Ions Life Sci.* **6**, 53–114.

Matthews, R. G., Koutmos, M. & Datta, S. (2008). *Curr. Opin. Struct. Biol.* **6**, 658–666.

Morris, R. J., Zwart, P. H., Cohen, S., Fernandez, F. J., Kakaris, M., Kirillova, O., Vonrhein, C., Perrakis, A. & Lamzin, V. S. (2004). *J. Synchrotron Rad.* **11**, 56–59.

Mueller, U., Darowski, N., Fuchs, M. R., Förster, R., Hellmig, M., Paithankar, K. S., Pühringer, S., Steffien, M., Zocher, G. & Weiss, M. S. (2012). *J. Synchrotron Rad.* **19**, 442–449.

Murshudov, G. N., Skubák, P., Lebedev, A. A., Pannu, N. S., Steiner, R. A., Nicholls, R. A., Winn, M. D., Long, F. & Vagin, A. A. (2011). *Acta Cryst.* D**67**, 355–367.

Nicholls, A. & Honig, B. (1991). *J. Comput. Chem.* **12**, 435–445.

Panjikar, S., Parthasarathy, V., Lamzin, V. S., Weiss, M. S. & Tucker, P. A. (2005). *Acta Cryst.* D**61**, 449–457.

Panjikar, S., Parthasarathy, V., Lamzin, V. S., Weiss, M. S. & Tucker, P. A. (2009). *Acta Cryst.* D**65**, 1089–1097.

Pejchal, R. & Ludwig, M. L. (2005). *PLoS Biol.* **3**, e31.

Perrakis, A., Morris, R. & Lamzin, V. S. (1999). *Nature Struct. Biol.* **6**, 458–463.

Pettersen, E. F., Goddard, T. D., Huang, C. C., Couch, G. S., Greenblatt, D. M., Meng, E. C. & Ferrin, T. E. (2004). *J. Comput. Chem.* **25**, 1605–1612.

Phillips, J. D., Whitby, F. G., Kushner, J. P. & Hill, C. P. (2003). *EMBO J.* **22**, 6225–6233.

Rocchia, W., Alexov, E. & Honig, B. (2001). *J. Phys. Chem. B*, **105**, 6507–6514.

Sauer, K. & Thauer, R. K. (1997). *Eur. J. Biochem.* **249**, 280–285.

Sauer, K. & Thauer, R. K. (2000). *Eur. J. Biochem.* **267**, 2498–2504.

Schneider, T. R. & Sheldrick, G. M. (2002). *Acta Cryst.* D**58**, 1772–1779.

Sheldrick, G. M. (2008). *Acta Cryst.* A**64**, 112–122.

Tallant, T. C., Paul, L. & Krzycki, J. A. (2001). *J. Biol. Chem.* **276**, 4485–4493.

Terwilliger, T. C. (2000). *Acta Cryst.* D**56**, 965–972.

Vagin, A. & Teplyakov, A. (2010). *Acta Cryst.* D**66**, 22–25.

Vaguine, A. A., Richelle, J. & Wodak, S. J. (1999). *Acta Cryst.* D**55**, 191–205.

Walden, H. (2010). *Acta Cryst.* D**66**, 352–357.

Weiss, M. S. (2001). *J. Appl. Cryst.* **34**, 130–135.
Winn, M. D. *et al.* (2011). *Acta Cryst.* D**67**, 235–242.
Wu, C. H., Yeh, L.-S. L., Huang, H., Arminski, L., Castro-Alvear, J., Chen, Y., Hu, Z., Kourtesis, P., Ledley, R. S., Suzek, B. E., Vinayaka, C. R., Zhang, J. & Barker, W. C. (2003). *Nucleic Acids Res.* **31**, 345–347.
Yang, A. S., Gunner, M. R., Sampogna, R., Sharp, K. & Honig, B. (1993). *Proteins*, **15**, 252–265.